

1 Title

2 Quantifying the impact of small boats on Posidonia seagrass meadows: methods and path
3 for future efficient management of anchoring pressure
4

5 Authors

6 Thomas Bockel^{1,2}, Noémie Bossut⁵, Nicolas Mouquet^{2,3}, David Mouillot², Quentin Fontaine⁴,
7 Julie Deter^{1,2}
8

9 ¹ Andromède océanologie, 7 place Cassan, Carnon plage, 34130 Mauguio, France

10 ² MARBEC, UMR IRD-CNRS-UM-IFREMER 9190, Université Montpellier, 34095 Montpellier
11 Cedex, France

12 ³ FRB - CESAB, Institut Bouisson Bertrand. 5, rue de l'École de médecine, 34000
13 Montpellier, France

14 ⁴ STARESO, Pointe Revellata, BP33, 20260 Calvi

15 ⁵ LAMSADE, UMR CNRS 7243, Université Paris Dauphine-PSL, 75775 Paris, France
16

17 Corresponding author :

18 Thomas Bockel

19 Andromède océanologie, 7 place Cassan, Carnon plage, 34130 Mauguio, France

20 thomas.bockel@andromede-ocean.com
21

22 Data availability

23 Data will be made available upon request.

24

25 Acknowledgements

26 The authors would like to thank all participants to data acquisition and/or analysis, in
27 particular Pierre Boissery from Agence de l'eau Rhône Méditerranée Corse and the Air
28 Attack company for providing data from the Medobs campaigns, Ignacio Pita from Marbec
29 research unit for his precious advices on the proper usage of SUMO, Thibault Catry from IRD
30 for his help in obtaining Pleiades images, and all the staff and interns at Andromède
31 Océanologie for their help.

32

33 Authors contribution

34 TB realized the analysis and wrote the scientific paper. NB helped with data analysis and
35 data collection. NM helped designing the research question and interpreting the results. DM
36 and QF provided part of the data for this work. JD supervised the work, helped designing the
37 research question and interpreting the results. All authors helped improving the manuscript.

38

39 Funding

40 This work is part of Thomas Bockel's Phd work funded by Agence Nationale pour la
41 Recherche (ANR), France Relance and Andromède océanologie (convention ANR-21-

42 PRRD-0102-01) in collaboration with UMR MARBEC and Université de Montpellier (research
43 collaboration contract n° 211672).

44 Part of the data acquisition (camera images from the alga bay) were funded by Stareso,

45 Collectivité de Corse and Agence de l'eau Rhône Méditerranée Corse as part of the

46 STARECAPMED project.

47

1 Abstract

2 Coastal ecosystems are exposed to anthropogenic pressures worldwide. Seagrass are
3 sensitive to human activities, especially through physical stress. Among them, boats induce
4 many pressures including physical degradation through anchoring. Mapping the anchoring
5 pressure of large boats (≥ 24 m) can be done with traditional methods but is still challenging
6 for smaller boats. Thus, the impact of large boats on coastal ecosystems is better
7 documented and more efficiently regulated in comparison with small ones.

8 Here, we characterize the pressure and the impact of boats anchoring on *Posidonia*
9 *oceanica* seagrass beds through the proxy of three landscape indices and compare
10 anchoring surveillance methods.

11 We show that small boats also have an impact on *P. oceanica* when anchoring.

12 AIS (Automatic identification System) and low resolution satellite imagery are poorly adapted
13 to detect small boats anchoring.

14 High resolution satellite imagery is a very efficient tool suitable even for small boats
15 detection, but is for now limited to punctual surveys due to its high costs.

16 We propose an automatic detection/localization tool adapted to multisource imagery and test
17 it successfully on a case study in Corsica (France).

18 Overall our study provides key quantified elements for the design of future efficient
19 surveillance and management of anchoring pressure.

20

21 Keywords

22 Seagrass, pressure monitoring, mooring, small ships, image analysis, satellite, AIS

23

24 Introduction

25 Coastal ecosystems, including mangroves, near shore reef ecosystems and
26 seagrass beds, are among the most important ecosystems not only ecologically, but also
27 economically and socially (Martínez et al. 2007; Barbier et al. 2011). Those sensitive
28 ecosystems are severely and increasingly threatened worldwide by human activities
29 (Halpern et al. 2008, 2015) including shipping (Halpern et al. 2019), which is responsible for
30 pollution and physical damage with anchoring (Deter et al. 2017).

31 Mapping anchoring pressure was traditionally performed by manual counts of boats, from a
32 boat, from shore, on fixed camera images (Bonhomme et al. 2013; Schohn et al. 2019), or
33 from airplanes during aerial survey (Holon et al. 2015; Serra-Sogas et al. 2021; MEDOBS
34 2024).

35 Since 2004, the automatic identification system (AIS) device is mandatory on ships of 300
36 gross tonnage and upwards (IMO 2018). This electronic transponder, communicating the
37 ship position and characteristics to surrounding receiving stations, allowed huge progress in
38 mapping large boats (≥ 24 m) anchoring events (Deter et al. 2017; Pergent-Martini et al.
39 2022; Bockel et al. 2023). AIS is however missing part of the small boats (Serra-Sogas et al.
40 2021).

41 Other methods like synthetic aperture radar (SAR) (Greidanus et al. 2017) or optical
42 (Kanjir et al. 2018) satellite imagery combined with efficient image analysis software such as
43 SUMO for SAR images, are also used to detect large boats (≥ 24 m) anchoring events. The
44 ever increasing resolution of satellite imagery has recently made it possible to achieve
45 impressive performance in ship detection, even on small boats (Jialeng et al. 2023).

46 Smartphones and social networks are another huge source of image data (Toivonen et al.
47 2019) that could also potentially be useful to map anchoring pressure whatever the boat
48 size.

49 Recent developments in artificial intelligence (AI) and especially deep learning
50 (LeCun et al. 2015; Wu et al. 2020) already allowed massive improvements in detection and

51 classification on satellite imagery (Goswami et al. 2020), with applications for boats
52 monitoring (Kanjir et al. 2018; Patel et al. 2022; Paolo et al. 2024).

53

54 The mediterranean sea is crossed by intense maritime traffic (March et al. 2021) and
55 a mecca for pleasure craft (Carreño and Lloret 2021). This implies considerable pressures
56 for its great biological diversity, with more than 17000 marine species and a very high rate of
57 endemism (20-30 %) (Coll et al. 2010; UNEP/MAP). The endemic species *Posidonia*
58 *oceanica* forms a protected key habitat hosting a high number of species and providing
59 many services (Boudouresque et al. 2012). *P. oceanica* seagrass beds are very sensitive to
60 anthropogenic threats (Boudouresque et al. 2009) and 70 % of its habitat is projected to be
61 lost by 2050 (Intergovernmental Panel on Climate Change (IPCC) 2022).

62 Large boats (≥ 24 m) anchoring highly impacts *Posidonia oceanica* meadows
63 (Boudouresque et al. 2012; Deter et al. 2017; Pergent-Martini et al. 2022). Few existing local
64 studies also suggest an impact from small boats (Francour et al. 1999; Milazzo et al. 2004;
65 Rouanet et al. 2013). Anchoring impacts on *P. oceanica* meadows are traditionally
66 characterized by large scars visible on aerial imagery for small depth (< 10 m deep) and
67 sonar imagery for deeper areas (Pasqualini et al. 1999) but can also be derived from
68 patterns observed in landscape indices. The decline index (proportion of living meadow) and
69 the patch cohesion index (characterizing the cohesion of the meadow) are the landscape
70 indices describing the conservation status of the meadow that best correlated with
71 anthropogenic pressures in the literature (Holon et al. 2018; Houngnandan et al. 2020). Their
72 application to characterize the conservation status of *Posidonia* seagrass beds, coupled to a
73 map of the anchoring pressure of large boats (≥ 24 m) (Deter et al. 2017), has led to a
74 tightening of regulations in France (Deter et al. 2022), regulations which have effectively
75 reduced these pressures in return (Bockel et al. 2023). Many questions now arise for smaller
76 boats: where do they anchor? To what extent do they impact when anchoring? What
77 methods are best suited to monitor the anchoring pressure of small boats?

78 The aim of this work was to address these questions. We first investigated the impact of
79 large and small boat anchoring on the French *Posidonia oceanica* meadows using the
80 proxies of landscape indices and AIS anchoring positions. We then compared AIS with the
81 other traditional methods used to monitor anchoring pressure. We proposed a new detection
82 and localization tool based on images from different sources and AI and tested it on a case
83 study in Corsica. We finally showed the relevance of high-resolution satellite imagery for
84 detecting small boats at anchor, and discussed the design of efficient anchoring surveillance.
85

86 Material and methods

87 1) Impact of boat anchoring on *Posidonia oceanica* 88 meadows, using AIS

89 1-1) Anchoring events and duration from AIS positions

90 AIS data were collected from two different sources. AIS data from 2010 to 2018 were
91 collected from Marine traffic database (www.marinetraffic.com). Those AIS positions
92 correspond to positions of declared anchoring activity, received by terrestrial AIS stations,
93 with an hourly frequency. AIS data from 2019 to 2022 came from the terrestrial receiving
94 stations of AIShub network (www.aishub.net) and from the vesselfinder database
95 (www.vesselfinder.com). Those AIS data are raw positions that were collected with a
96 frequency of one position every two minutes. All AIS data contain information on boat
97 identification and size, time of detection, geographic coordinates, heading direction, speed,
98 dimensions, type, and destination (when declared). All AIS positions were combined in a
99 unique database independently of source or frequency.

100 The methodology used to obtain the anchoring positions from AIS (approx. 55·000
101 between 2010 and 2018 and approx. 160·000 between 2019 and 2022) was derived from the
102 work of Deter et al. (2017) and Bockel et al. (2023). Briefly, a boat was considered at anchor
103 when its successive AIS positions (at least four) had low speed (< 1 kt) and were stationary
104 (distance between points \leq 600 m). A regression circle was then fitted on those positions to
105 calculate the anchoring polygon.

106 Cumulated anchoring duration was calculated on 100 x 100 m cells for big boats (\geq
107 24 m) on one part and small boats (< 24 m) on another part. For each boat size category, a
108 pixel was labeled as “anchoring” if anchored only by boats belonging to the size category or
109 smaller.

110 1-2) Landscape indices from the biocenoses map

111 Landscape indices were calculated for *Posidonia oceanica* (Houngnandan et al.
112 2020) based on the 2023 update of the 1/10000 map of the marine biocenoses in the entire
113 French Mediterranean sea between 0 and 80 m deep (Andromède Océanologie 2014)
114 (www.medtrix.fr, donia expert project). Biocenoses data was rasterized at a resolution of 5 m
115 before calculating the three following landscape indices: decline index, patch cohesion index
116 and landscape division index. Formulas for each index were reported in **Error! Reference**
117 **source not found..** The landscape indices were calculated in 100 x 100 m cells using the R
118 software 4.2.1 and the packages SDMTools 1.1-221.2 and terra 1.6-17.

119 1-3) Analysis

120 Values of each landscape index were calculated and plotted on areas with and
121 without small or large boat anchoring and the differences were tested using a Wilcoxon test.
122 Very shallow areas (< 5 m deep) and the deepest areas (> 30 m deep) were removed from
123 this analysis, to avoid landscape patterns outside of the anchoring bathymetric range to
124 influence the results.

125

126 2) Comparison of AIS and other traditional methods used to 127 map anchoring

128 This analysis was realized on a study area covering the Medobs and Sentinel 1 SAR
129 acquisition areas in the French Mediterranean sea within a period covering the summer of
130 2020. Areas and dates of acquisitions for Medobs, AIS and Sentinel 1 SAR are reported in
131 **Error! Reference source not found.** and **Error! Reference source not found.**

132 2-1) AIS

133 AIS-derived anchoring events were mapped as described above.

134 2-2) Sentinel 1 SAR images and SUMO

135 Sentinel 1 SAR images were downloaded from NASA EARTHDATA ASF data platform
136 (search.asf.alaska.edu). L1 Detected High-Res Single-Pol (GRD-HS) sentinel products were
137 used. Sentinel 1 images (n = 13) were analyzed using the Search for Unidentified Maritime
138 Objects (SUMO) software (Greidanus et al. 2017). Cross-polarization and co-polarization
139 detection threshold adjustments were applied based on the literature (Galdelli et al. 2021;
140 Pita et al. 2022). No land buffer was used. Coordinates and estimated size of each detected
141 boat were obtained.

142 2-3) Medobs

143 Medobs (MEDOBS 2024) is a monitoring network of human activities using aerial
144 surveillance on the French Mediterranean coast. Operated by the Air Attack Technologies
145 company and funded by the Agence de l'eau Rhône Méditerranée Corse (French water
146 agency), this network includes multiple aerial surveys of the entire coastline including
147 Corsica, with a higher density of flights during summer. Boats are manually counted and

148 regrouped by anchoring zones (hotspots of anchoring) and size classes (< 10 m: small; 10 -
149 24 m: medium; ≥ 24 m: large). Thirteen survey dates and 1068 anchoring zones were
150 analyzed for the 2020 summer.

151 2-4) Analysis

152 For each Medobs anchoring zone, the number of boats detected by Medobs and by
153 AIS/SAR were compared. In order to filter out zones out of AIS/SAR detection ranges, only
154 Medobs anchoring zones containing AIS detections/SAR detections were kept for this
155 analysis. Sentinel 1 SAR images were acquired by the satellite at two different timeframes: 5
156 am or 5 pm. Boat detections on 5 am images were considered as boats anchored since the
157 day before the detection. The mean percentages of “medobs boats” detected by AIS and
158 SAR for each size class were calculated. The difference of detection performance between
159 size classes and detection methods were tested using a Wilcoxon test.

160

161 3) Terrestrial and aerial imagery to better map anchoring 162 boats

163 A suite of tools was developed to detect any type and size of boats on multisource
164 imagery, and to localize their position based on the metadata of the images.

165 3-1) Images dataset

166 The dataset of images (344 images) was composed of two main types of images
167 (figure S2). The first type of images (71 % of the images) is multisource images:
168 smartphones and drones images taken by our team (Andromède océanologie) during the
169 summer in 2022 and 2023, fixed camera on the coast ([Stareso](#), summer 2020) and aerial
170 images (Medobs, summer 2022). The second type of images (29 % of the images) were

171 downloaded from an opensource boats images dataset (Bogue Sound Team Roboflow
172 2023).
173 All images were randomly separated between training set (83 %), test set (7 %) and
174 validation set (10 %). Labeling of boats on images before training was performed with the
175 online application Make Sense (Skalski 2019) and was semi supervised (all images were
176 pretreated with YOLOv5 and then checked visually and corrected manually when needed).

177 3-2) YOLOv8 detection algorithm and its improvement

178 The boat detection algorithm was trained using YOLOv8 on a GPU equipped server.
179 Although initially planned with 500 epochs to ensure comprehensive learning, the training
180 was concluded after approximately 300 epochs due to satisfactory performance metrics
181 achieved earlier than expected. This early stopping helps prevent overfitting while
182 maintaining high accuracy. Images were automatically resized to a standard size of 640 by
183 640 pixels to facilitate uniform processing.

184 3-3) Localization methodology

185 The developed localization tool was entirely based on the metadata of the image.
186 Image metadata are encrypted in image files in Exif format (Exchangeable Image File
187 Format). They contain information on the image shot, essential for localization: date,
188 coordinates, altitude, camera captor width and focal length, angles of the shot (pitch, yaw
189 and roll), and image height and width (in pixels). Some devices such as drones contained
190 very complete image metadata, but others such as smartphones contained metadata of
191 variable quality, often lacking several parameters. In this case, precise localization was only
192 possible when the photographer manually provided missing parameters, at least date,
193 coordinates of the camera and yaw angle. Camera captor width and focal length could be
194 inferred from the camera model, roll was assumed to be 0 (the localization tool doesn't work
195 otherwise), altitude could be inferred from the coordinates and freely accessible digital

196 elevation models, and pitch was assumed to be linearly linked to the height of the relative
197 horizon in the image (pitch of 0 for a relative horizon of 0.5 and pitch of -30° for a relative
198 horizon of 1) using the following formula: $\text{pitch}(p) = (-60 * \text{relative horizon}) - 30$.

199 Using basic principles of trigonometry (Figure 1), the boat real position was then
200 derived from its relative position in the image (rel_x and rel_y , defined at the middle bottom
201 of the detection bounding box) using the following equations:

202

$$203 \quad \text{phiXh} = \text{atan}((Sh * (\text{abs}(\text{rel}_x) * 2)) / Cf / 2)$$

$$204 \quad \text{phiYh} = \text{atan}((Sh * (\text{image height} / \text{image width}) * (\text{abs}(\text{rel}_y) * 2)) / Cf / 2)$$

205

206 *if boat on top half of image (y coordinate in image < 0.5):*

$$207 \quad K = A / (\tan(-p) - \text{phiYh})$$

208 *if boat on bottom half of image:*

$$209 \quad K = A / (\tan(-p) + \text{phiYh})$$

210

$$211 \quad R = \text{sqr}t(A^2 + K^2)$$

212

213 *if boat on right half of image (x coordinate in image > 0.5):*

$$214 \quad W = R * \tan(\text{phiXh})$$

215 *if boat on left half of image:*

$$216 \quad W = -(R * \tan(\text{phiXh}))$$

217

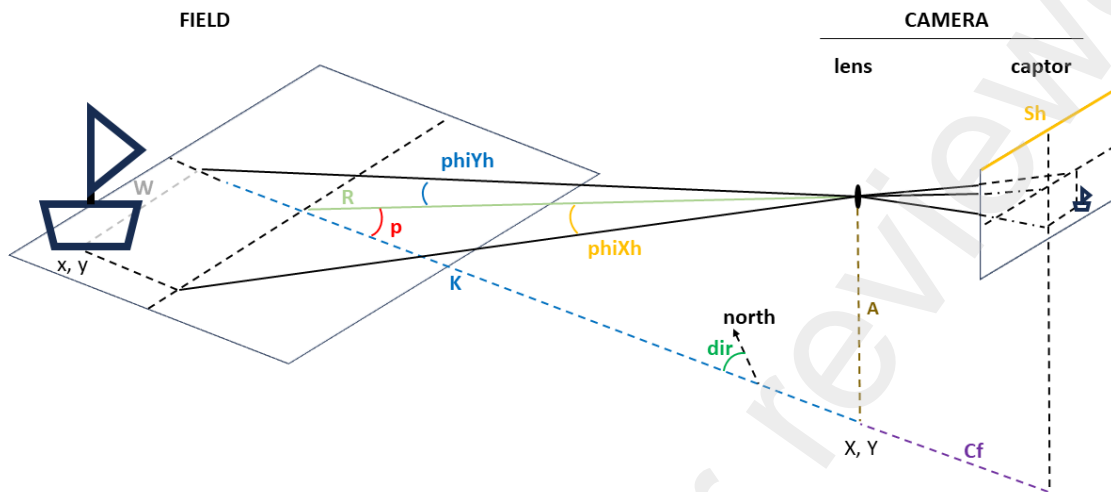
$$218 \quad x = X + W * \cos(\text{dir}) + K * \sin(\text{dir})$$

$$219 \quad y = Y - W * \sin(\text{dir}) + K * \cos(\text{dir})$$

220

221 A filter was then applied to consider the low reliability of localization near the edges of the
222 image or near the relative horizon. Only boats detected in the 99 % of the image farthest

223 from the image edges (or from the relative horizon when shot not vertical and altitude < 10
224 m) were kept.



225
226 *Figure 1 Schematic view of localization method. Boat position on the field (left) is derived from boat position on*
227 *the camera image (right), using camera metadata (captor width S_h and focal length C_f) and field metadata*
228 *(altitude A and coordinates X and Y of the camera, angles of the shot (dir and p), and distance K to the target.*

229

230 3-4) Performance analysis of detection and sensitivity analysis of 231 localization

232 The performance of the detection model was evaluated by calculating its average
233 precision (proportion of true positive detections among all positive detections) and recall
234 (proportion of true positive detections among all actual positive ones) and by comparing
235 between the YOLOv8 standard algorithm using default YOLO coco weights, and our
236 YOLOv8 custom algorithm trained on our images dataset.

237 The performance of the localization tool was evaluated by running a sensitivity
238 analysis on a separate subset of images where the true location of the detected boat was
239 known. The error between the true position and the estimated position was calculated. Each

240 factor potentially influencing this localization error was extracted from the images: distance
241 between boat and camera, altitude, method of acquisition (smartphone or drone), relative
242 position of the boat with respect to the horizon on the image, relative position of the boat with
243 respect to the center of the image, and relative position of the horizon. A linear regression
244 was performed to assess the relationship between each factor and the localization error
245 (previously log-transformed for normality).

246 3-5) Application of the custom YOLO detection and localization 247 methodology to the case study of the Alga bay

248 The « Alga » bay, located north of the city of Calvi in Corsica (France), was equipped
249 with a Bushnell 30MP CORE Trail Camera, positioned at an altitude of 89 m in order to
250 cover the entire bay. Photographs were acquired every hour during daylight for the summer
251 period of 2020. The first exploitable image every morning (8 am) was considered the most
252 representative of the boats anchored during the night and extracted from the database.
253 Those images (n = 62) were then processed through our custom detection localization
254 algorithm (**Error! Reference source not found., Error! Reference source not found.**).
255 The depth category was extracted for each detection using a bathymetric raster produced by
256 combining the best available resolution between SHOM data, and Andromède océanologie
257 bathymetric dataset; categories were defined as follows: deeper than -20 m, -20 to -10 m,
258 and shallower than -10 m. The average number of boats detected per night and depth
259 category was calculated and compared with anchoring boats detected during the same night
260 based on AIS data using the method described above. The difference between both
261 methods was tested using a Wilcoxon comparison test.

262

263 4) High resolution optical satellite imagery to better map 264 anchoring boats

265 A pre-trained YOLOv8 detection algorithm was tested on high resolution optical satellite
266 imagery to detect small boats at anchor.

267

268 4-1) Images and pretreatment

269 The images used were Airbus Pleiades multispectral (2 m resolution) and
270 panchromatic (50 cm resolution) on a study area of 17 km width and 13 km height centered
271 on the area of Bonifacio and the Lavezzi islands in south Corsica. Images were available at
272 three timestamps: 2023/07/19 at 10:31 am, 2023/07/26 at 10:28 am, and 2023/08/14 at
273 10:31 am. The 2023/07/26 image was removed from the analysis because the numerous
274 waves negatively affected the YOLO detection performances.

275 Images were pansharpened and tiled at a size of 1000 by 1000 pixels using gdal 3.0.4. An
276 overlap of 100 pixels was used during tiling in order not to remove any boats from the
277 database. Tiles containing shallow water areas (0 – 20 m deep) were extracted for boats
278 detection.

279

280 4-2) YOLO detection and validation

281 YOLOv8 base weights were obtained from a pre-training performed on a google
282 earth dataset (Cole Robin 2023). Boats detection was performed on each previously created
283 tile using YOLOv8 and the obtained base weights, with an automatic resizing of the tiles to a
284 standard size of 640 by 640 pixels (**Error! Reference source not found.**). A sample of 100
285 tiles per image, with the associated detections, was then used to create a reference
286 annotation dataset using Roboflow (Dwyer et al. 2024) online annotation tool (774 boats

287 annotated for the 2023/08/14 image and 670 boats annotated for the 2023/07/19 image).
288 YOLOv8 algorithm using base weights was then retrained using the 2023/07/19 reference
289 dataset as training set, and 2023/08/14 reference dataset as validation set. Boat detections
290 on land or inside ports were filtered out. Precision and recall metrics were then calculated for
291 each boat size class (0-5m, 5-10m, 10-15m, >15m).

292

293 Results

294 1) Impact of boat anchoring using AIS

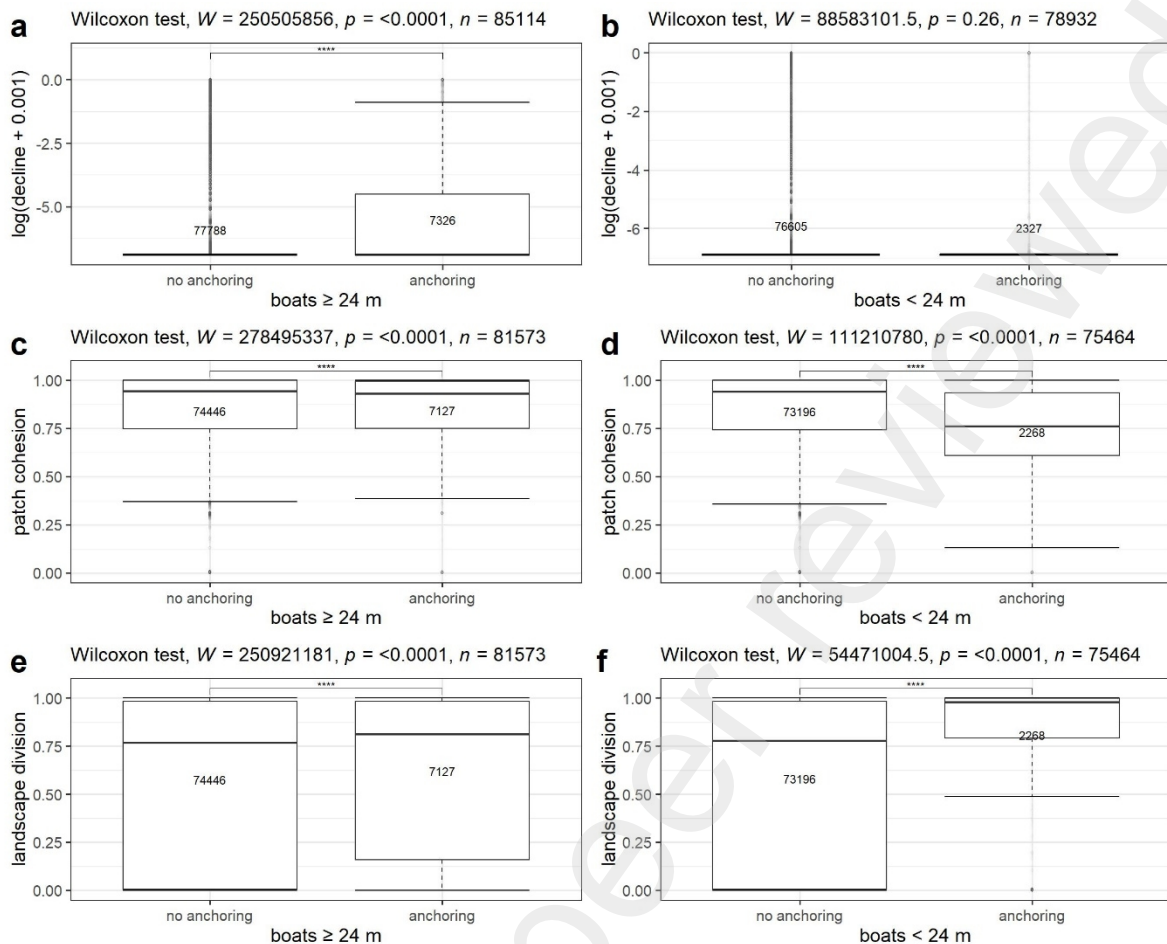
295 The anchoring dataset contained 225°470 anchoring polygons between 2010 and 2022
296 (129°552 for large boats (≥ 24 m) and 95°918 for small boats (< 24 m)). Cumulated
297 anchoring duration calculation gave a total of 23 092 100 m x 100 m cells with anchoring
298 (11°235 containing anchoring of only large boats and 3°389 containing anchoring of only
299 small boats).

300 The decline index was significantly higher on areas with large boat anchoring
301 compared to areas without large boat anchoring ($W = 2.5 \cdot 10^8$, $p < 0.001$, $n = 85^\circ 114$), and
302 not significantly different between areas with or without small boat anchoring ($W = 8.9 \cdot 10^7$, p
303 > 0.1 , $n = 78^\circ 932$) (Figure 2).

304 The patch cohesion index was significantly lower on areas with anchoring compared
305 to areas without anchoring; for large boats ($W = 2.8 \cdot 10^8$, $p < 0.001$, $n = 81^\circ 573$), and for
306 small boats ($W = 1.1 \cdot 10^8$, $p < 0.001$, $n = 75^\circ 464$) (Figure 2).

307 The landscape division index was significantly higher on areas with anchoring
308 compared to areas without anchoring; for large boats ($W = 2.5 \cdot 10^8$, $p < 0.001$, $n = 81^\circ 573$),
309 and for small boats ($W = 5.5 \cdot 10^7$, $p < 0.001$, $n = 75^\circ 464$) (Figure 2).

310



311

312 *Figure 2 Statistical distribution of landscape indices for each size category of ais boats (≥ 24 m or < 24 m) with or*
 313 *without anchoring. a. log(decline index) (boats ≥ 24 m), b. log(decline index) (boats < 24 m), c. patch cohesion*
 314 *index (boats ≥ 24 m), d. patch cohesion index (boats < 24 m), e. landscape division index (boats ≥ 24 m), f.*
 315 *landscape division index (boats < 24 m). Numbers inside the bars indicate the number of 100 x 100 m cells where*
 316 *each indicator was calculated (this number is higher for the decline index compared to the other indices because*
 317 *also taking into account dead matte).*

318

319

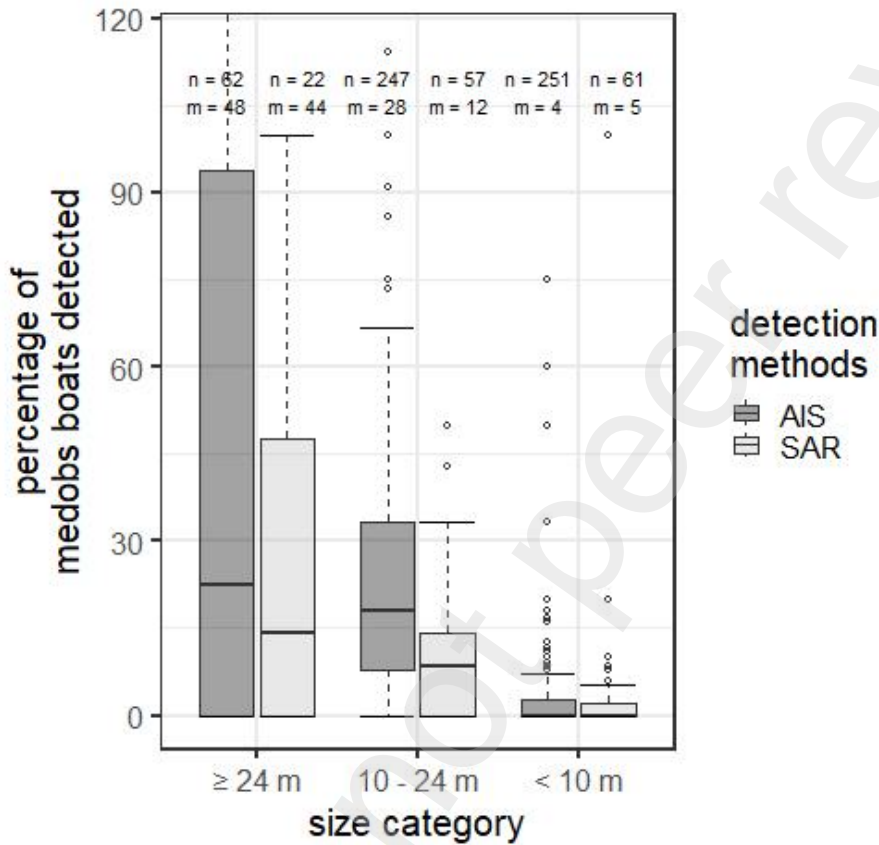
320 2) Comparison of AIS and other traditional methods used to

321 map anchoring

322 Differences between size classes, for both detection methods, were significant only between

323 large (≥ 24 m) and small boats (< 10 m) (AIS: $W = 1.1 \cdot 10^3$, $p < 0.001$, $n = 313$; SAR: $W = 9.6$

324 10^2 , $p < 0.001$, $n = 83$) and between medium (10 – 24 m) and small boats (AIS: $W = 5.2 \cdot 10^4$,
 325 $p < 0.001$, $n = 498$; SAR: $W = 2.4 \cdot 10^3$, $p < 0.001$, $n = 118$) with larger boats being more
 326 detected than small ones (Figure 3). Differences between detection methods were significant
 327 only for medium boats ($W = 9.7 \cdot 10^3$, $p < 0.001$, $n = 304$) with more boats detected on
 328 average by AIS (28 % of Medobs observations) than by SAR (12 %) (Figure 3).



329

330 *Figure 3 Mean percentage of Medobs boats detected by AIS and SAR, for each size category (≥ 24 m, 10 - 24 m,*

331 *< 10 m; n = number of Medobs anchoring zones, m = mean percentage of Medobs boats detected).*

332

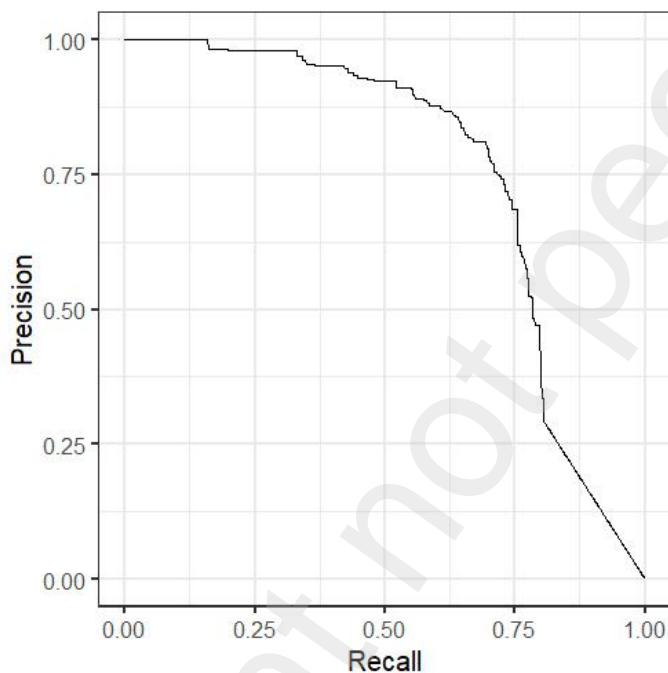
333 3) Terrestrial and aerial imagery to better map anchoring

334 boats

335 3-1) Performances of the detection algorithm and improved model

336 On the validation dataset, YOLOv8 showed an average precision of 0.63 and an
337 average recall of 0.42. The improved custom model showed an average precision of 0.81
338 and an average recall of 0.69. The custom model presents a good balance between
339 precision and recall (Figure 4, **Error! Reference source not found.**).

340



341

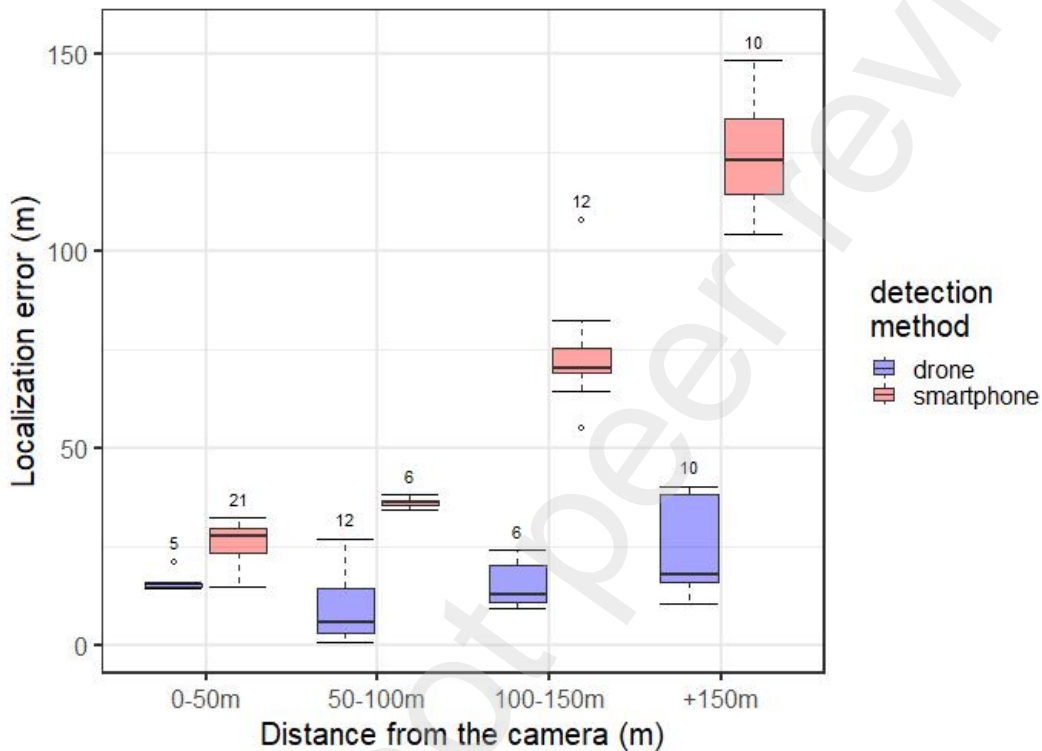
342 *Figure 4 Precision recall curve for the custom detection model*

343

344 3-2) Localization performances and sensitivity analysis

345 The linear regression between the images metadata and the logarithm of the
346 localization error explained 73 % of the variance of the localization error ($F = 51$, $p < 0.001$,
347 adjusted $R^2 = 0.73$). The localization error was significantly negatively influenced by altitude

348 (t = -3.8, p < 0.001) and significantly positively influenced by the method (t = 2.2, p < 0.05)
 349 and the distance between the boat and the camera (t = 10, p < 0.001). The average
 350 localization error under ideal conditions (using the drone method with a distance between
 351 the boat and the camera below 200 meters) was 16 m (**Error! Reference source not**
 352 **found.** and Figure 5).
 353



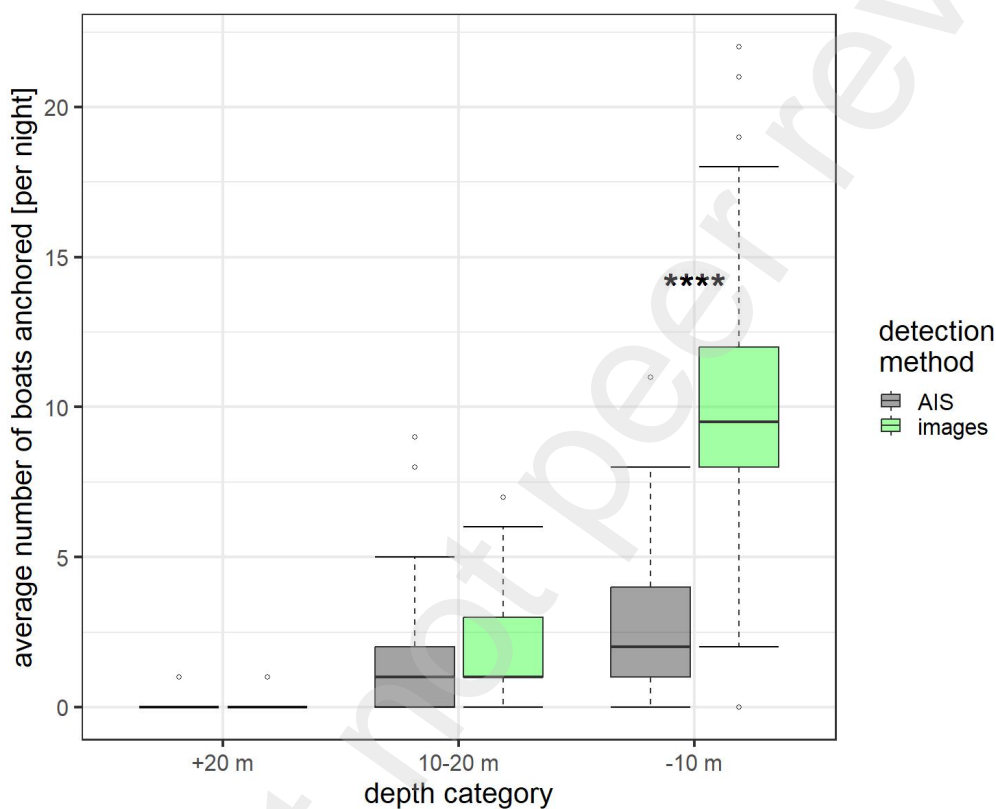
354
 355 *Figure 5 Error of the localization method as a function of the distance to the camera and the acquisition method*
 356 *(drone or smartphone). The number of images is indicated above each boxplot.*

357
 358 3-3) Application of the YOLO detection and localization methodology to
 359 the case study of the Alga bay (Corsica)

360 The average number of detected anchored boats per night and detection method
 361 was equal to 0.032 (AIS) and 0.05 (images) for depth below 20 m; 1.6 (AIS) and 1.8
 362 (images) for depth between 10 m and 20 m; and 2.7 (AIS) and 10 (images) for depth above

363 10 m (Figure 6). The average number of anchored boats detected per night increased
364 significantly with decreasing depth, for both methods ($W < 1221$, $p < 0.001$, $n = 62$). The
365 number of anchored boats detected per night was significantly higher for images than AIS at
366 a shallow depth (- 10 m) ($W = 240$, $p < 0.001$, $n = 62$). The differences between images and
367 AIS were not significant for the other depth categories (10-20m: $W = 1669$, $p > 0.1$, $n = 62$;
368 +20m: $W = 1891$, $p > 0.1$, $n = 62$) (Figure 6).

369



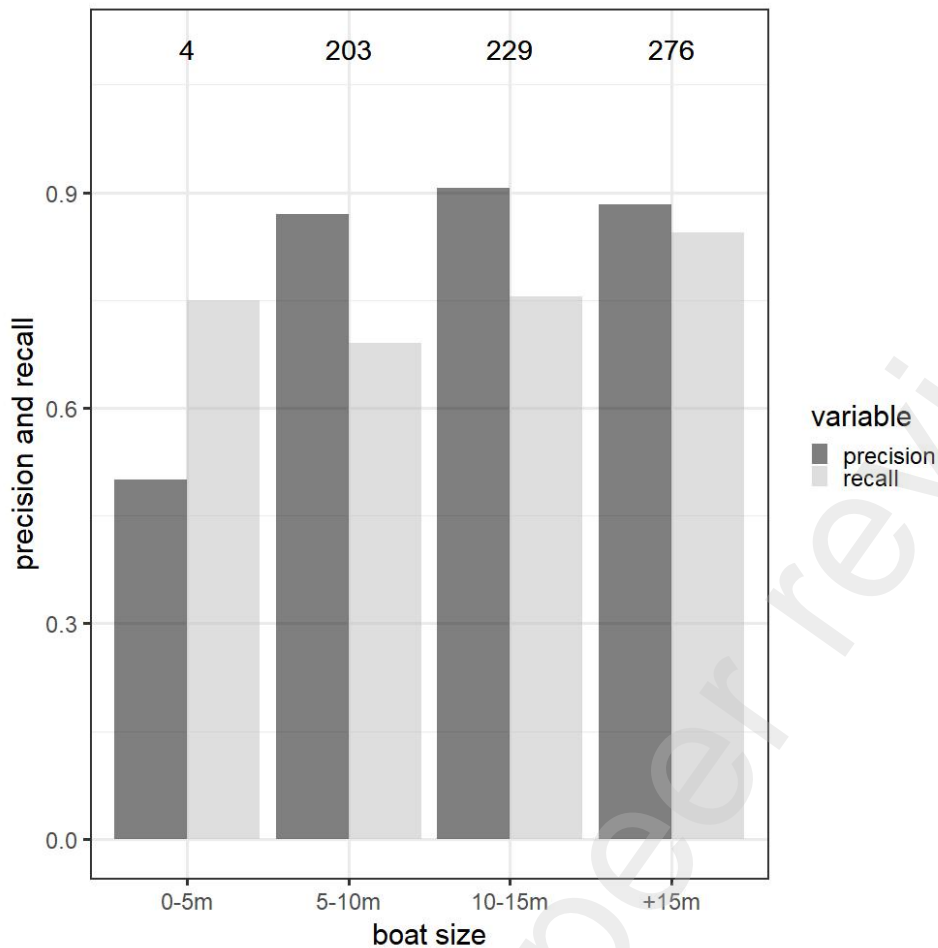
370

371 *Figure 6 Average number of boats detected at anchoring per night, for each depth category and detection*
372 *method*

373

374 4) High resolution optical satellite imagery to better map
375 anchoring boats

376 Post-training of YOLOv8 base algorithm using 2023/07/19 training dataset did not
377 improve the performance of the detection algorithm on the 2023/08/14 validation dataset.
378 Average precision on the validation dataset was equal to 0.91, and average recall was equal
379 to 0.77. Precision vs recall, precision vs confidence and recall vs confidence curves were
380 reported in **Error! Reference source not found.** After filtering out detections on land and
381 inside ports, average precision values per size class were equal to 0.5 (0-5m), 0.87 (5-10m),
382 0.91 (10-15m), 0.88 (>15m), and average recall values per size class were equal to 0.75 (0-
383 5m), 0.69 (5-10m), 0.76 (10-15m), 0.84 (>15m).
384 While recall values were relatively high and constant for each boat size class, precision
385 value was 43 % lower for boats smaller than 5 m compared to boats longer than 5 m. This
386 value is to be interpreted with caution as only four boats smaller than 5 m were present in
387 the dataset.



388

389 *Figure 7 Precision and recall metrics per size class of YOLOv8 algorithm on optical satellite imagery. Numbers at*
 390 *the top indicate the number of boats per size class*

391

392 Discussion

393 1) Impact of boat anchoring using AIS

394 The impact of large boats ($\geq 24\text{m}$) anchoring was confirmed on each analyzed landscape
 395 indices (decline, patch cohesion and landscape division) for *Posidonia oceanica* meadows.

396 Moreover, small boats detected by AIS ($< 24\text{ m}$) are also responsible for measurable
 397 impacts: patch cohesion index and landscape division index were significantly degraded in
 398 presence of small boats anchoring. Small boats damage the spatial configuration of the

399 meadows when anchoring, and these changes in configuration could be an early warning of
400 future decline, not yet detected. Scars induced by small boats anchoring in the meadow
401 could also be too narrow to be detected as dead matte during lateral sonar acquisitions,
402 explaining the absence of significant impact on the decline index.

403 The impact of small boats is detected even though their number is underestimated due
404 to the rare presence of AIS equipment on small boats (Greidanus et al. 2017; Paolo et al.
405 2024) (see 2 Comparison of AIS and other traditional methods used to map anchoring). It is
406 therefore necessary to monitor those anchoring events, whether or not the boats are
407 equipped with AIS, because they are not currently affected by the French regulation
408 prohibiting anchoring in *P. oceanica* seagrass beds. This more detailed knowledge
409 depending on the size is all the more important as the number of boats, including small
410 boats, continues to increase, particularly in protected marine areas, and requires monitoring
411 to address carrying capacity issues (Gómez et al. 2023).

412

413 2) From the comparison of AIS and other traditional methods 414 to the test of terrestrial and aerial imagery to better map 415 anchoring boats

416 This study demonstrated both at the scale of the French Mediterranean sea and at the
417 scale of a bay, that AIS data, while allowing to detect a general pattern of impact, are poorly
418 adapted to a detailed mapping of small boats anchoring impacts, in accordance with the
419 literature (Serra-Sogas et al. 2021).

420 Similarly, freely available low resolution (10 m) SAR satellite imagery was shown to be
421 poorly adapted to detect small boats (only 12 % of small Medobs boats (10 - 24 m) and 5 %
422 of very small boats (< 10 m) detected on SAR S1 images during summer 2020), in
423 accordance with the literature (Greidanus et al. 2017).

424 As Medobs images cannot be acquired continuously and automatically, alternative
425 methods must be proposed. Using multi-source images, the image-based tool developed in
426 this work showed very good detection (average precision of 0.81 and average recall of 0.69)
427 and localization (average localization error of 16 m under ideal conditions) performances.
428 Some limitations must however be kept in mind under certain conditions such as very low
429 altitude (below 2 m) and/or large distance to targets (above 2 km) and the presence of
430 detection artefacts (important sun reflections at the sea surface, presence of buoys). Most of
431 these limitations can however be controlled when using fixed cameras with well known
432 acquisition metadata (see below).

433 The case study of the Alga bay showed a very similar rate of detection by AIS and
434 the camera for areas deeper than -10 m but many anchoring were missed by AIS compared
435 to the camera for areas shallower than -10 m. These anchoring events at such shallow
436 depths most probably correspond to the smallest boats. The absence of an estimation of the
437 boat size is a limitation of the image-based method, but this information could be calculated
438 if the wind conditions are known at the date of acquisition of the image, and if the camera
439 line of sight is perpendicular to the dominant wind in the area. The camera should be placed
440 at a minimal altitude of approximately five meters in order to obtain an acceptable
441 localization error for boats as far as approximately one kilometer from the camera. The
442 automatic camera detection localization tool is moreover flexible and adapted to any source
443 of terrestrial or aerial imagery (smartphone, drone, small aircraft such as ultra-light motorized
444 planes (ULMs), or even webcams or social networks images), and provides automatic boat
445 detection and localization, allowing important time gains in data analysis. The image
446 acquisition represents a very low cost (approximately 400 euros for the purchase, installation
447 and usage of the camera).

448 This method is therefore perfectly adapted to implement high-frequency surveillance on
449 localized high-stake anchoring areas, and allows a detailed spatio-temporal reporting of
450 large and small boats anchoring pressure, as well as an estimation of the total frequentation
451 and turnover of boats on the surveyed sites.

452

453 3) High resolution satellite optical imagery to better map 454 anchoring boats

455 The YOLO detection algorithm tested in this work on Pleiades images showed very good
456 performances (average precision of 0.91 and average recall of 0.77), close to the
457 performances of the pretraining reference work (precision of 0.94 and recall of 0.93) (Cole
458 Robin 2023), and very good compared to other recent studies (accuracy of 0.94 and
459 precision of 0.74 (Jialeng et al. 2023), and accuracy of 0.99 and precision of 0.84 (Patel et
460 al. 2022)). While recall values were relatively high and constant, precision appeared to
461 decrease by more than 40 % for boats smaller than five meters. This pattern could indicate a
462 good reliability of the detection algorithm only for boats longer than five meters, but is to be
463 interpreted with caution as only four boats smaller than five meters were present in the
464 dataset. Waves, small private swimming pools, and very high density of boats next to each
465 other (ports) were visually observed as factors negatively influencing the detection algorithm
466 performances. Those factors can however easily be filtered out during images pre-selection
467 and detections post-treatment.

468 Satellite imagery field is evolving very fast and higher resolution (e.g. Pleiades neo (30 cm
469 resolution) for optical imagery (Soubirane 2019)) is already available. High resolution
470 satellite imagery, as well as aerial surveys, are very appropriate for punctual monitoring to
471 get a rough idea of the pressure, but their important costs make those methods less
472 appropriate for regular surveillance.

473

474 Conclusion and future path for management

475 This work confirmed the impact of large boats (≥ 24 m) anchoring on *Posidonia*
476 *oceanica* meadows using three different landscape indices (decline, patch cohesion and
477 landscape division), and showed that small boats (< 24 m) anchoring, despite very low
478 accuracy detection by AIS, also seem to have an impact on *P. oceanica* meadows (impact
479 detected on two of three analyzed indices: patch cohesion and landscape division). This
480 work demonstrated that traditional monitoring methods such as AIS and low resolution freely
481 available SAR satellite images, while detecting a reasonable part of large boats (≥ 24 m,
482 approximately 50 %) are poorly adapted to small (10 – 24 m, approximately 20 %) and very
483 small boats (< 10 m, approximately 5 %) detection.

484 The strong suitability of high-resolution satellite imagery for small boats automatic detection
485 was demonstrated but must be reserved, for the time, for punctual monitoring because of the
486 relatively high costs involved. This work then proposed an automatic detection localization
487 tool based on multi-sources images, and tested it successfully on a case study in Corsica.
488 This tool is particularly adapted to high-frequency localized monitoring and could be easily
489 deployed by harbourmasters and marine areas managers that could make appropriate use
490 of existing images or set up an automatic image-taking system. With constantly improving
491 technologies, it can be a struggle for managers to balance the pros and cons of each
492 monitoring solution. The perfect solution does not exist, and addressing managers specific
493 needs will inevitably involve a mix between the previously mentioned solutions. Well-
494 designed monitoring and surveillance plans will both allow the construction of adapted
495 management plans and enable managers to control and evaluate their efficiency. This work
496 provides key quantified elements for the design of future efficient surveillance and
497 management of anchoring pressure.

498

499 References

- 500 Andromède Océanologie (2014) Les dessous de la mer méditerranée—Cartographie de la
501 méditerranée française au 1/100000ème. Publi int Agence de l'eau RMC. 2014.
502 Available:
503 http://www.eaurmc.fr/fileadmin/documentation/brochures_d_information/Mer_Mediterranee/Livret_Surfstat-WEB.pdf
504
- 505 Barbier EB, Hacker SD, Kennedy C, et al (2011) The value of estuarine and coastal
506 ecosystem services. *Ecological Monographs* 81:169–193. [https://doi.org/10.1890/10-](https://doi.org/10.1890/10-1510.1)
507 1510.1
- 508 Bockel T, Marre G, Delaruelle G, et al (2023) Anchoring pressure and the effectiveness of
509 new management measures quantified using AIS data and a mobile application.
510 *Marine Pollution Bulletin* 195:115511.
511 <https://doi.org/10.1016/j.marpolbul.2023.115511>
- 512 Bogue Sound Team Roboflow (2023) BogueSound_BoatDetection Dataset. In: Roboflow.
513 [https://universe.roboflow.com/bogue-sound-team-](https://universe.roboflow.com/bogue-sound-team-roboflow/boguesound_boatdetection)
514 [roboflow/boguesound_boatdetection](https://universe.roboflow.com/bogue-sound-team-roboflow/boguesound_boatdetection). Accessed 7 Feb 2024
- 515 Bonhomme P, Bonhomme D, Frachon N (2013) A METHOD FOR ASSESSING
516 ANCHORING PRESSURE. In: *Rapp. Comm. int. Mer Médit.*, 40, 2013
- 517 Boudouresque, Bernard, Bonhomme, et al (2012) Protection and conservation of *Posidonia*
518 *oceanica* meadows. RAMOGE - RAC/SPA
- 519 Boudouresque CF, Bernard G, Pergent G, et al (2009) Regression of Mediterranean
520 seagrasses caused by natural processes and anthropogenic disturbances and
521 stress: a critical review. *52:395–418*. <https://doi.org/10.1515/BOT.2009.057>

- 522 Carreño A, Lloret J (2021) Environmental impacts of increasing leisure boating activity in
523 Mediterranean coastal waters. *Ocean & Coastal Management* 209:105693.
524 <https://doi.org/10.1016/j.ocecoaman.2021.105693>
- 525 Cole Robin (2023) Kaggle ships in satellite imagery with YOLOv8. GitHub repository.
526 <https://github.com/robmarkcole/kaggle-ships-in-satellite-imagery-with-YOLOv8>
- 527 Coll M, Piroddi C, Steenbeek J, et al (2010) The Biodiversity of the Mediterranean Sea:
528 Estimates, Patterns, and Threats. *PLOS ONE* 5:e11842.
529 <https://doi.org/10.1371/journal.pone.0011842>
- 530 Deter J, Bockel T, Delaruelle G, et al (2022) Préservation des posidonies: les ressorts d'une
531 collaboration efficace. In: sfecologie.org. [https://sfecologie.org/regard/r104-juin-2022-](https://sfecologie.org/regard/r104-juin-2022-j-deter-et-al-posidonies/)
532 [j-deter-et-al-posidonies/](https://sfecologie.org/regard/r104-juin-2022-j-deter-et-al-posidonies/). Accessed 10 Dec 2022
- 533 Deter J, Lozupone X, Inacio A, et al (2017) Boat anchoring pressure on coastal seabed:
534 Quantification and bias estimation using AIS data. *Marine Pollution Bulletin* 123:175–
535 181. <https://doi.org/10.1016/j.marpolbul.2017.08.065>
- 536 Dwyer B, Nelson J, Hansen T, et al. (2024) Roboflow
- 537 Francour P, Ganteaume A, Poulain M (1999) Effects of boat anchoring in *Posidonia*
538 *oceanica* seagrass beds in the Port-Cros National Park (north-western
539 Mediterranean Sea). *Aquatic Conservation Marine and Freshwater Ecosystems*
540 9:391–400. [https://doi.org/10.1002/\(SICI\)1099-0755\(199907/08\)9:43.0.CO;2-8](https://doi.org/10.1002/(SICI)1099-0755(199907/08)9:43.0.CO;2-8)
- 541 Galdelli A, Mancini A, Ferrà C, Tasseti AN (2021) A Synergic Integration of AIS Data and
542 SAR Imagery to Monitor Fisheries and Detect Suspicious Activities. *Sensors*
543 21:2756. <https://doi.org/10.3390/s21082756>

- 544 Gómez AG, Balaguer P, Fernández-Mora À, Tintoré J (2023) Mapping the nautical carrying
545 capacity of anchoring areas of the Balearic Islands' coast. *Marine Policy* 155:105775.
546 <https://doi.org/10.1016/j.marpol.2023.105775>
- 547 Goswami N, Kathiriya K, Yadav S, et al (2020) Satellite Imagery Classification with Deep
548 Learning : A Survey. *International Journal of Scientific Research in Computer
549 Science, Engineering and Information Technology* 36–46.
550 <https://doi.org/10.32628/CSEIT2065124>
- 551 Greidanus H, Alvarez M, Santamaria C, et al (2017) The SUMO Ship Detector Algorithm for
552 Satellite Radar Images. *Remote Sensing* 9:246. <https://doi.org/10.3390/rs9030246>
- 553 Halpern BS, Frazier M, Afflerbach J, et al (2019) Recent pace of change in human impact on
554 the world's ocean. *Sci Rep* 9:11609. <https://doi.org/10.1038/s41598-019-47201-9>
- 555 Halpern BS, Frazier M, Potapenko J, et al (2015) Spatial and temporal changes in
556 cumulative human impacts on the world's ocean. *Nature Communications* 6:7615.
557 <https://doi.org/10.1038/ncomms8615>
- 558 Halpern BS, Walbridge S, Selkoe KA (2008) A Global Map of Human Impact on Marine
559 Ecosystems. *Science* 319:946–948. <https://doi.org/10.1126/science.1151084>
- 560 Holon F, Marre G, Parravicini V, et al (2018) A predictive model based on multiple coastal
561 anthropogenic pressures explains the degradation status of a marine ecosystem:
562 Implications for management and conservation. *Biological Conservation* 222:125–
563 135. <https://doi.org/10.1016/j.biocon.2018.04.006>
- 564 Holon F, Mouquet N, Boissery P, et al (2015) Fine-Scale Cartography of Human Impacts
565 along French Mediterranean Coasts: A Relevant Map for the Management of Marine
566 Ecosystems. *PLOS ONE* 10:e0135473. <https://doi.org/10.1371/journal.pone.0135473>

567 Houngnandan F, Kéfi S, Deter J (2020) Identifying key-conservation areas for Posidonia
568 oceanica seagrass beds. *Biological Conservation* 247:108546.
569 <https://doi.org/10.1016/j.biocon.2020.108546>

570 IMO (2018) Automatic Identification Systems (AIS). In:
571 <https://www.imo.org/en/OurWork/Safety/Pages/AIS.aspx>.
572 <http://www.imo.org/en/ourwork/safety/navigation/pages/ais.aspx>. Accessed 19 Oct
573 2018

574 Intergovernmental Panel on Climate Change (IPCC) (ed) (2022) Changing Ocean, Marine
575 Ecosystems, and Dependent Communities. In: *The Ocean and Cryosphere in a*
576 *Changing Climate: Special Report of the Intergovernmental Panel on Climate*
577 *Change*. Cambridge University Press, Cambridge, pp 447–588

578 Jialeng G, Suárez de la Fuente S, Smith T (2023) BoatNet: automated small boat
579 composition detection using deep learning on satellite imagery. *UCL Open Environ*
580 *5:e058*. <https://doi.org/10.14324/111.444/ucloe.000058>

581 Kanjir U, Greidanus H, Oštir K (2018) Vessel detection and classification from spaceborne
582 optical images: A literature survey. *Remote Sensing of Environment* 207:1–26.
583 <https://doi.org/10.1016/j.rse.2017.12.033>

584 LeCun Y, Bengio Y, Hinton G (2015) Deep learning. *Nature* 521:436–444.
585 <https://doi.org/10.1038/nature14539>

586 March D, Metcalfe K, Tintoré J, Godley BJ (2021) Tracking the global reduction of marine
587 traffic during the COVID-19 pandemic. *Nat Commun* 12:2415.
588 <https://doi.org/10.1038/s41467-021-22423-6>

589 Martínez ML, Intralawan A, Vázquez G, et al (2007) The coasts of our world: Ecological,
590 economic and social importance. *Ecological Economics* 63:254–272.
591 <https://doi.org/10.1016/j.ecolecon.2006.10.022>

592 MEDOBS (2024) MEDOBS. https://medtrix.fr/portfolio_page/medobs/. Accessed 28 Nov
593 2018

594 Milazzo M, Badalamenti F, Ceccherelli G, Chemello R (2004) Boat anchoring on *Posidonia*
595 *oceanica* beds in a marine protected area (Italy, western Mediterranean): effect of
596 anchor types in different anchoring stages. *Journal of Experimental Marine Biology*
597 *and Ecology* 299:51–62. <https://doi.org/10.1016/j.jembe.2003.09.003>

598 Paolo F, Kroodsma D, Raynor J, et al (2024) Satellite mapping reveals extensive industrial
599 activity at sea. *Nature* 625:85–91. <https://doi.org/10.1038/s41586-023-06825-8>

600 Pasqualini V, Pergent-Martini C, Pergent G (1999) Environmental impact identification along
601 the Corsican coast (Mediterranean sea) using image processing. *Aquatic Botany*
602 65:311–320. [https://doi.org/10.1016/S0304-3770\(99\)00048-0](https://doi.org/10.1016/S0304-3770(99)00048-0)

603 Patel K, Bhatt C, Mazzeo PL (2022) Deep Learning-Based Automatic Detection of Ships: An
604 Experimental Study Using Satellite Images. *Journal of Imaging* 8:182.
605 <https://doi.org/10.3390/jimaging8070182>

606 Pergent-Martini C, Monnier B, Lehmann L, et al (2022) Major regression of *Posidonia*
607 *oceanica* meadows in relation with recreational boat anchoring: A case study from
608 Sant'Amanza bay. *Journal of Sea Research* 188:102258.
609 <https://doi.org/10.1016/j.seares.2022.102258>

610 Pita I, Seguin R, Shin Y-J, et al (2022) SAR Satellite Imagery Reveals the Impact of the
611 Covid-19 Crisis on Ship Frequentation in the French Mediterranean Waters. *Front*
612 *Mar Sci* 9:. <https://doi.org/10.3389/fmars.2022.845419>

613 Rouanet E, Astuch P, Bonhomme D, et al (2013) EVIDENCE OF ANCHOR EFFECT IN A
614 POSIDONIA OCEANICA SEAGRASS MEADOW UNDER LOW ANCHORING
615 PRESSURE VIA A MULTI-CRITERIA GRID

616 Schohn T, Astruch P, Rouanet E (2019) Innovative management tools to survey boat traffic
617 and anchoring activities within a marine protected area. Planning, nature and
618 ecosystem services. <https://doi.org/10.6093/978-88-6887-054.6>

619 Serra-Sogas N, O'Hara PD, Pearce K, et al (2021) Using aerial surveys to fill gaps in AIS
620 vessel traffic data to inform threat assessments, vessel management and planning.
621 Marine Policy 133:104765. <https://doi.org/10.1016/j.marpol.2021.104765>

622 Skalski P (2019) SkalskiP/make-sense

623 Soubirane J (2019) Shaping the Future of Earth Observation with Pléiades Neo. In: 2019 9th
624 International Conference on Recent Advances in Space Technologies (RAST). pp
625 399–401

626 Toivonen T, Heikinheimo V, Fink C, et al (2019) Social media data for conservation science:
627 A methodological overview. Biological Conservation 233:298–315.
628 <https://doi.org/10.1016/j.biocon.2019.01.023>

629 UNEP/MAP Biological diversity in the Mediterranean.
630 <https://www.unep.org/unepmap/resources/factsheets/biological-diversity>. Accessed 8
631 Feb 2024

632 Wu X, Sahoo D, Hoi SCH (2020) Recent advances in deep learning for object detection.
633 Neurocomputing 396:39–64. <https://doi.org/10.1016/j.neucom.2020.01.085>

634